Activity report of the Italian CRG beamline at the European Synchrotron Radiation Facility (ESRF)

N 10, Jan 2023

Grenoble, Jan 2023

71 Avenue des Martyrs, Grenoble, France

Responsabile editoriale: Francesco d'Acapito (*dacapito@iom.cnr.it*)

Editing: Francesco d'Acapito

ISSN 2553-9248

DOI: 10.5281/zenodo.7436673

Keywords

Italian beamline at ESRF, BM08

LISA project

X-ray Absorption Spectroscopy

Contents

Foreword

During year 2022, LISA has resumed the user activities free from sanitary restrictions. Full teams of scientists had the opportunity to carry out experiments "*in presence*" for the first time since the start of the EBS operation. 29 experiments, 15 on the ESRF quota and 14 on the CERIC quota, have been carried out with a total number of shifts dedicated to the users of 436 out of which 223 for ESRF and 213 for CERIC. Figure 1 presents some statistical data relative to the experiments carried out at LISA this year:

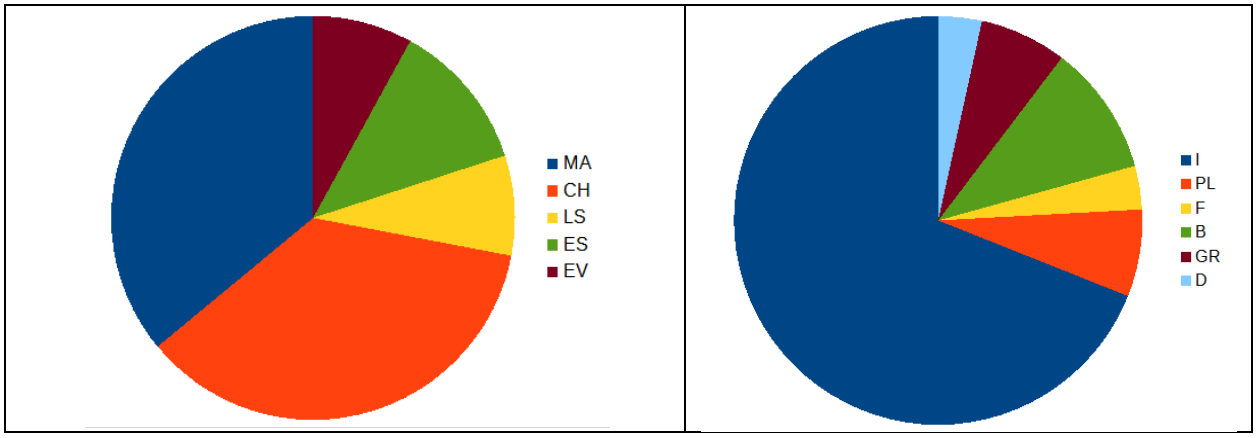

Figure 1: Statistical data about experiments carried out at LISA. Left: Scientific areas. Right: Nationality of the main proposers.

The left panel of Figure 1 shows the scientific areas covered by the users, showing a marked predominance of Materials and Engineering (MA) and Chemistry (CH) and contributions from Earth Science (ES), Life sciences (LS), Environment (EV). The right panel of Figure 1 shows the nationality of the main proposers: Italy accounts for approximately 2/3 of the total but significant contributions come from Poland and Belgium. Users from Germany, France and Greece are also present.

During this year, several scientists have worked at the beamline: Michela Brunelli and Malik Rehman during the first semester whereas Alessandro Puri joined back the staff in the second semester. In addition, 4 PhD students have spent some months at LISA learning the bases of x-ray absorption spectroscopy and carrying out experiments with the users: Tommaso Baroni (Uni Firenze), Xiufang He (Uni Milano), Hao Chen (Politecnico Milano), Sara Massardo (Uni Genova).

Several technical developments concerned the data collection and management, with the adoption of the FAIR principles as implemented by the ESRF, the development of an online XAS extraction tool for evaluation during the collection and new methods of data collection in pump-and-probe modes. With the help of the IOM design office, we have conceived and realized a new cell for liquid samples, which now completes the portfolio of sample holders available for the users.

Turning to science, it is worth noticing that (photo-) (electro-) chemistry plays a dominant role with several experiments carried out in *operando* and *pump-and-probe* modes devoted to the comprehension of the structural and chemical changes at electrodes during voltammetric cycles and/or light illumination. In addition, studies in the cultural heritage field have started with particular attention to the depth sensitive mode obtained by collecting data at the same time in fluorescence and total electron yield mode. The possibility of carrying out experiments at high energy (> 40 keV), namely at the K edges of Rare Earth elements, has been particularly appreciated by the community.

For next year, the main challenge will be the replacement of SPEC as environment for the beamline management with BLISS following the example of the other ESRF beamlines. This will affect all the aspects of data collection and management of optical elements but we are confident to complete it with a minimum effect on the users' activity.

News from the beamline

Online XAS extraction

A software routine for the live extraction of XAS data during acquisitions (LivEstra), which was derived from the ESTRA-FitEXA software package [1], has been set up on the beamline acquisition PC and successfully tested. The routine recognizes the acquisition mode (transmission or fluorescence) and automatically runs on the spectrum being currently acquired, without any action required by the users or the local contact. For acquisitions with a multi-element detector, it first performs the average of the working fluorescence channels, excluding by default those counting less than 70% the average counts, or with noise level three times the average noise (the counts and noise level thresholds can be adjusted manually, if needed). The routine performs background subtraction and normalization, extracts the EXAFS signal and performs its Fourier transform (FT), estimates the noise of the data, and it shows the results graphically exploiting the Gnuplot software. Several default settings can be manually adjusted by editing a simple text file (e.g. columns to be read in the experimental file to account for non-standard acquisition modes, k-weight to be displayed for EXAFS signal, FT range and window width, pre-edge limits, degrees of the polynomials for noise calculations, etc.).

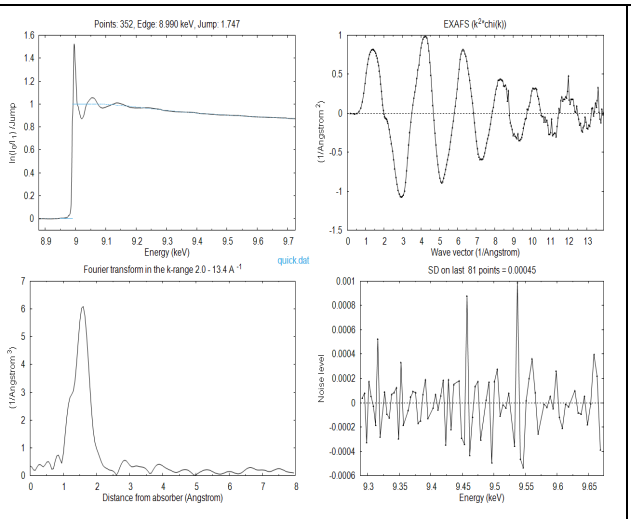

One of the main features of the routine is the optimization of the edge-step value, which is critical for a good extraction of the data. The edge-step optimization routine is based on the repeated calculation of the FT, decreasing or increasing the initial edge-step value by a certain percentage, until a minimum in the average of the values of the FT in the region 0 – 1 Angstrom (which do not contains physically relevant signal) is reached. The graphical output showing the extraction summary of the spectrum being acquired (Figure 1a) is shown on the data collection workstation.

Figure 2 Graphical output showing a summary of the EXAFS extraction for a transmission acquisition. In clockwise order: background-subtracted and normalized spectrum, k^2-weigthed EXAFS signal, noise level, FT amplitude of the EXAFS signal (not phase-corrected).

LivEstra easily allows also to non-experienced users to check the quality of the ongoing XAS acquisitions, preventing accidental waste of valuable beamtime.

[1] ESTRA-FitEXA: A software package for EXAFS data analysis. Meneghini, C., Bardelli, F., Mobilio, S. (2012) NIM-B **285**, 153-157.

Cell for liquid samples

A new cell for analyzing liquid samples at ambient conditions has been designed and tested and it is now available for users. The body is realized in PEEK (PolyEther Ether Ketone) whereas the windows are Kapton. The cell has a total volume of ~250 µl and the total channel length is ~ 20 mm. It is optimized for use at 45° for fluorescence measurements but it can as well be used in transmission geometry. Figure 3 shows the drawings of the cell and an example of spectrum collected

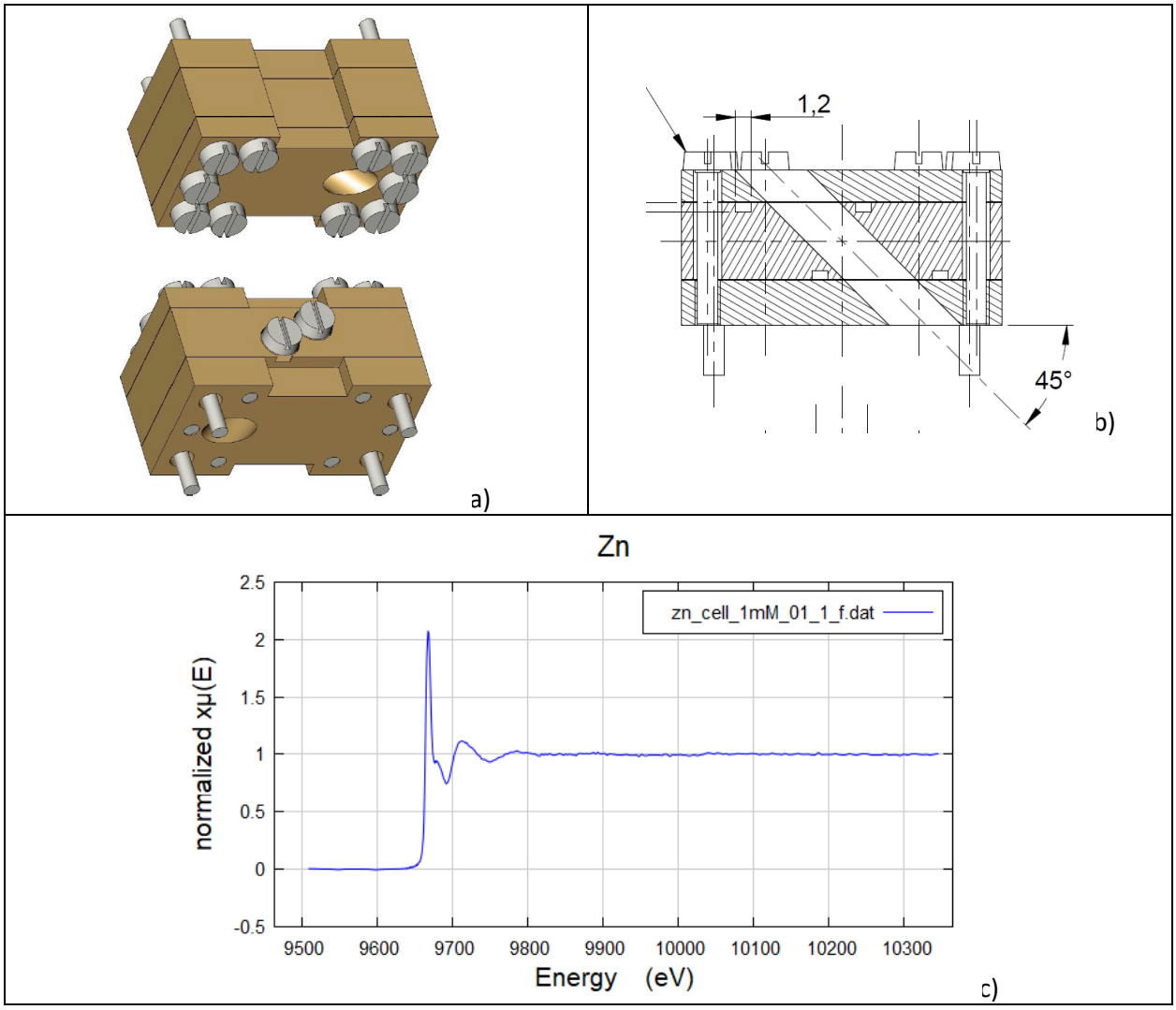

Figure 3; The cell for liquid samples. a) 3D views of the cell. b) side view showing the channel at 45°, c) example of a Zn-K edge XAS spectrum of 1mM $ZnSO_4$ in water collected with the cell.

Data and publication policies at LISA

Since the beginning of this year, LISA data are **F**indable **A**ccessible **I**nteroperable **R**eusable (FAIR). Following the framework put in place by the ESRF, now LISA data are stored in a central repository accessible via the site https://data.esrf.fr . Following the ESRF data policy recently adopted, all datasets generated from publicly funded research will receive a Digital Object Identifier (DOI) that the user must cite in the publications involving the data. Data are at exclusive use of the group that collected it during an embargo period of three years. Successively, unless the owners extend the embargo upon formal request, the data are made publicly available. Figure 4 shows some screenshots from the web page:

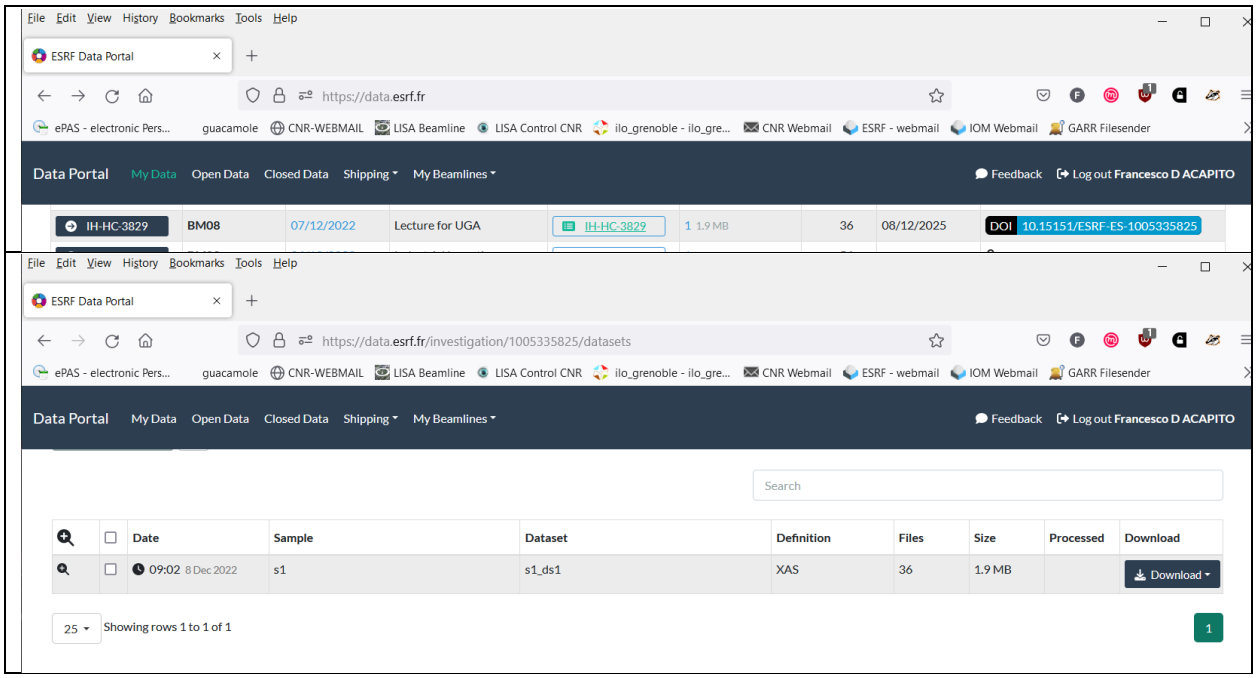

*Figure 4: **Up**: page of the data.esrf.fr site showing an experiment with the DOI. **Down**: page obtained by clicking on the field with the experiment name on the left with the field for downloading.*

The use of the DOI is part of the general policy of ESRF about publication of data generated on site that include a proper acknowledgement of the beamline the local contact and communication of the publication to the library. Concerning data collected at LISA, the beamline must always be cited with its main publication:

> *F. d'Acapito, G. O. Lepore, A. Puri, A. Laloni, F. La Manna, E. Dettona, A. De Luisa, A. Martin, "The LISA beamline at ESRF", Journal of Synchrotron Radiation 26 (2019) 551-558, https://doi.org/10.1107/S160057751801843X*

The general recommendations about data publications issued by the joint ESRF-ILL library are shown Figure 5:

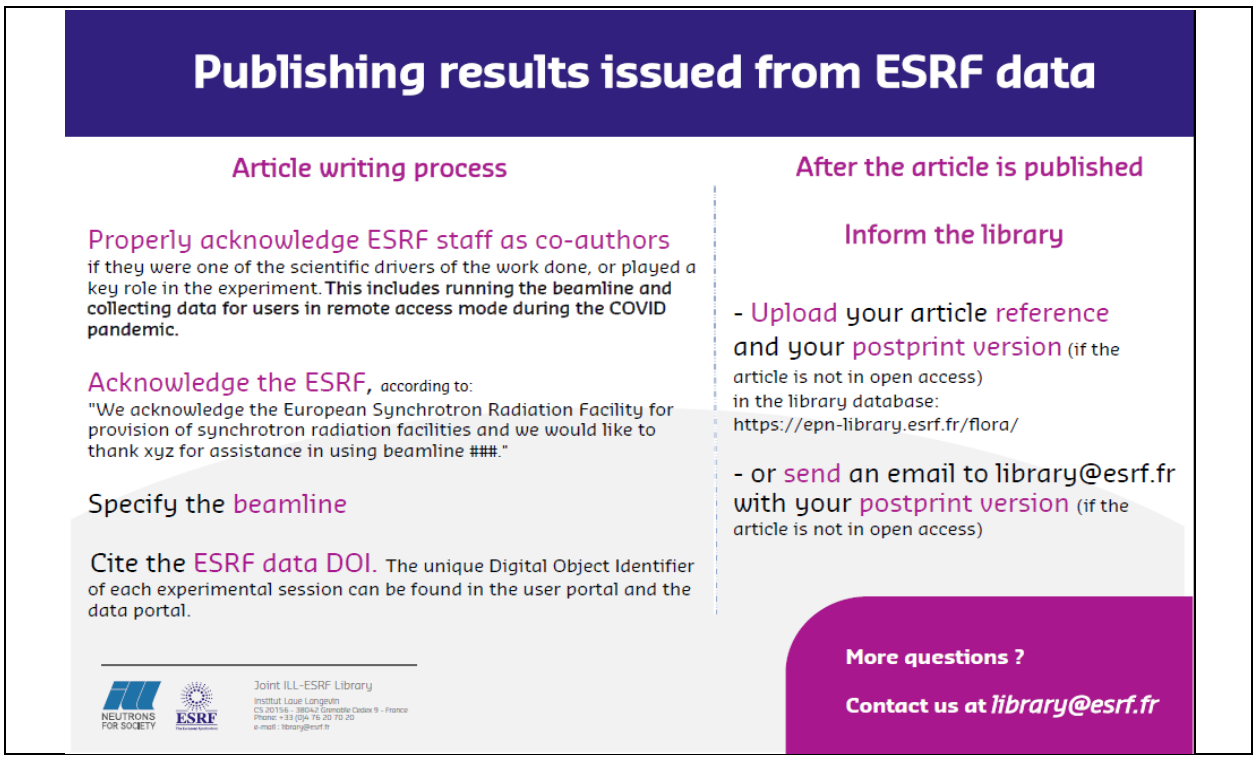

Figure 5: Recommendations for publication of data collected at ESRF.

Additional info are available in the ESRF site in the section dedicated to the data policy, https://www.esrf.fr/datapolicy and https://www.esrf.fr/UsersAndScience/UserGuide/Publications .

Improvement in pump & probe measurement algorithm.

An improved algorithm tailored for pump & probe measurements has been implemented at LISA. It allows time-gated point-by-point data acquisition triggering an external stimulus in order to compensate possible drifts in the acquisition setup over long-term measurements.

A dedicated python script with graphical user interface (see Figure 6) is now available for pump & probe data pre-treatment. It generates two user friendly data files one corresponding to spectrum with no external stimulus (_off) and the other to the spectrum with external stimulus (_on).

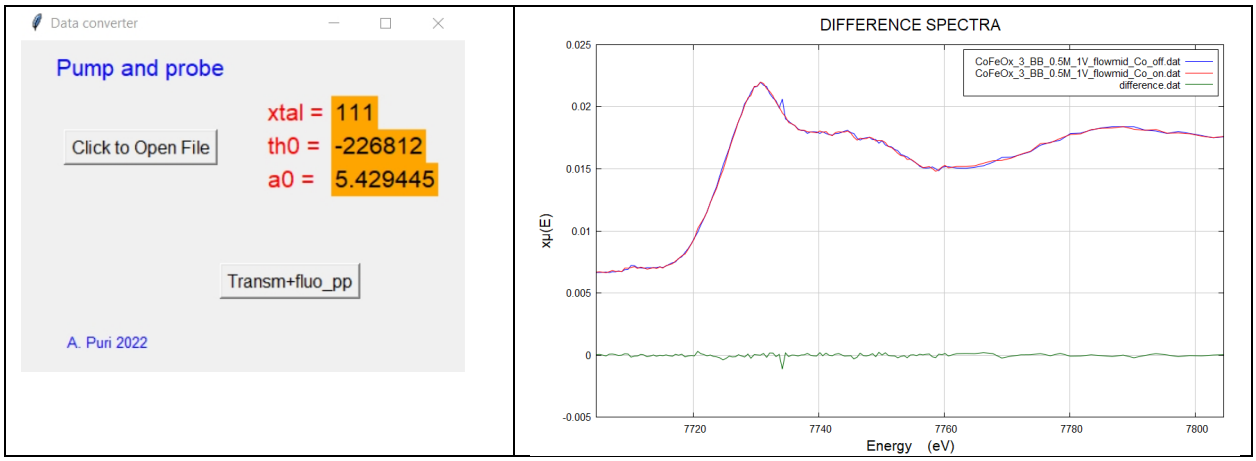

Figure 6: Left: GUI for pump & probe data pre-treatment. Right: Difference of spectra collected with and without visible light illumination of the sample obtained using the GUI (courtesy of Mazzaro et al. experiment CH-6417.)

Doctorate Students activity

Operando and Time-Resolved X-Ray Absorption Spectroscopy for Photoelectrochemical Water Splitting over Cu/Cu_xO

X. He[1], M. Fracchia[2], A. Vertova[1,3], A. Puri[4], F. d'Acapito[4], P. Ghigna[2], A. Minguzzi[1,3]

1. Dipartimento di Chimica, Università degli Studi di Milano, via Golgi, 19, 20133, Milano, Italy
2. Dipartimento di Chimica, Università di Pavia, Viale Taramelli 16, 27100, Pavia, Italy
3. Consorzio Interuniversitario Nazionale per la Scienza e Tecnologia dei Materiali – INSTM, Via G. Giusti 9, 50121, Firenze, Italy
4. CNR-Istituto Officina dei Materiali (IOM)-OGG, c/o ESRF-71, Avenue des Martyrs, 38043 Grenoble, France

Solving fossil fuel global energy dependence and its related environmental issues are some of the most urgent concerns. The adoption of renewable sources requires a method for storing energy, thus leveling the natural oscillatory nature of sunlight, winds, and wave. Storage is also required for the exploitation of energy for transportation. In this case, batteries are (and will) play the main role in small and medium size vehicles, but are not sustainable for larger ones (buses, ships). Hydrogen is the best alternative as an energy vector, but it must be synthetized from water with processes that do not produce CO_2 or other (greenhouse gases) emissions. This is the so-called green hydrogen. Photovoltaic panels-driven electrolysis cells can be used to store electric energy as H_2. In a future perspective, a direct conversion of sunlight to H_2 is welcomed, but it requires a device that simultaneously absorbs light, producing "hot" charges that oxidize/reduce a suitable chemical species, such as water [1]. This in turn motivates the search for new materials, based on abundant elements, that present semiconducting properties (to absorbs sunlight and convert it into photogenerated charges) and good catalytic properties towards hydrogen production (from water reduction). A good example is CuxO, a low-cost and environmentally friendly photoelectrode, whose activity has been already demonstrated by our group [2]. Recently, we improved the photoconversion capability of CuxO by inhibiting the charge recombination process, using a Cu thin underlayer deposited between the conductive glass (Fluorine-Tin Oxide (FTO)), and the CuxO layer.

Photogenerated charge dynamics is therefore a key factor for the improvement of any photoelectrode (and for Cu_xO in particular) and this at the basis of the present X-ray Absorption Spectroscopy time-resolved investigation. XAS already demonstrated its importance in studying (photo)electrodes, for its ability in determining the average oxidation state of a selected element and its local structure.

In this work, we carried out in-situ time pump&probe XAS investigations on $FTO/Cu/Cu_xO$ photocathodes, whose preparation was carried out in LISA chemical lab. To synthesize CuxO and Cu/CuxO, CuI was used as a precursor, and dispersed on FTO, while Cu foil underlayer was synthesized via electrochemical deposition method. After preparation, the samples were put in furnace (Nabertherm Controller P320) and heated in air.

To investigate the photo-induced electrons and holes transfer path over CuxO and Cu/CuxO on in-situ condition, we collected operando X-ray absorption near edge structure (XANES) spectra at the Cu-K edge. The cell consists of a standard 3-electrodes system: Pt foil (Counter electrode), Ag/AgCl (reference electrode), and coated FTO (working electrode), and pH 7 phosphate buffer solution (K_2HPO_4+KH_2PO_4) is used as electrolyte. A Biologic SP50 potentiostat is (kindly provided by the ESRF Electrochemistry Laboratory), was used to record the electrochemical signals during chronoamperometries and Cyclic

Voltammetries (CV). The potentiostat was controlled by its software "EC-LAB", that was remotely controlled.

XAS spectra were recorded in the 16 bunches mode, so that the distance between probes (X-ray bunches) is of 176 ns. We used 2 lenses to obtain a wide light angle. Three types of light sources were used as the source of UV-Vis light (Pump): a LED, a laser (400 nm), and a photodiode (400 nm). According to the light and dark chopped current of the same sample at the same applied potential, the photocurrent under photodiode is higher, which means the photodiode has the highest light intensity in our experiment. Pump and probe experiments were performed under Laser illumination, The time delay between laser pulse and X-ray can be controlled from 0 ns to 158 ns. Thus, we collected different CuxO and Cu/CuxO spectra with different time delays at different applied potentials. The light on and light off spectra can be collected simultaneously, to compare the differences in real time. Under photodiode illumination, we changed the applied potential and collected the spectra. XANES of CuxO is displayed in Figure 1. Under OCP condition, the CuxO illustrated typical CuO peak. When the applied potential is 0.3 V vs RHE, the shoulder located at 8978 eV becomes flat. While the shoulder located at 8986 eV is becoming more obvious, indicating CuxO reveals a mixture state of Cu_2O and CuO peak. Since from our previous experiment some differences in the pre-edge region existed, we also collected the Fixed-energy X-ray absorption voltammetry (FEXRAV) spectra under light and dark chopped conditions at fixed potential.

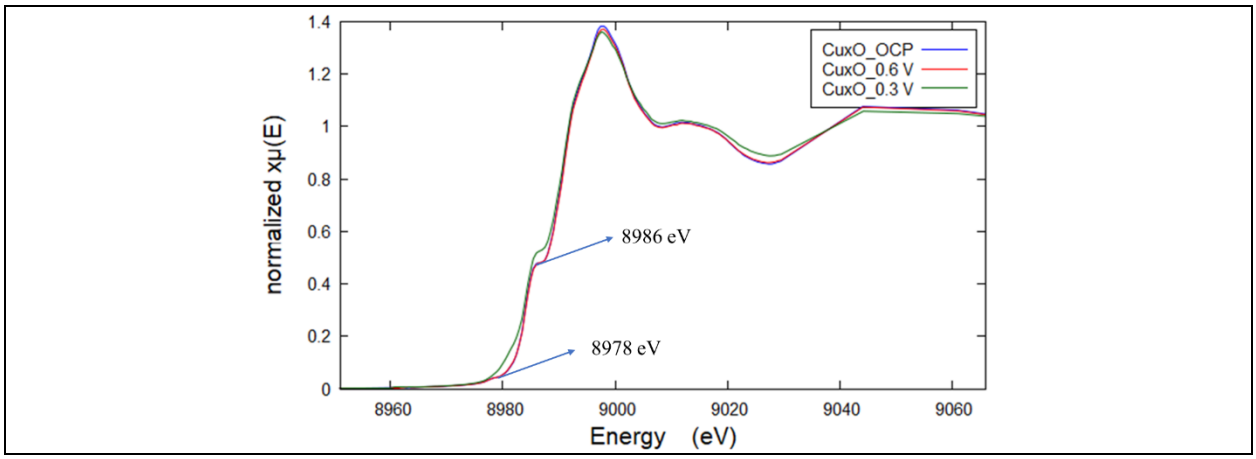

Figure 7: XANES of CuxO at different potential at Cu-K edge under photodiode illumination.

Reference:

1. C. Murugan and A. Pandikumar. *ACS Applied Energy Materials* **2022** *5* (6), 6618-6632

2. T. Baran, S. Wojtyła, C. Lenardi, A. Vertova, P. Ghigna, E. Achilli, M. Fracchia, S. Rondinini, and A. Minguzzi. *ACS Applied Materials & Interfaces* **2016** *8* (33), 21250-21260

A study of the defects architecture in co-doped ceria electrolytes for solid oxides cells

S. Massardo[1], C. Artini[1, 2], M.M. Carnasciali[1,3], A. Martinelli[4], F. d'Acapito[5], M. Pani[1,4]

[1]DCCI, University of Genova, Genova, Italy; [2]CNR-ICMATE, Genova, Italy; [3]INSTM, Genova, Italy; [4]SPIN-CNR, Genova, Italy; [5]IOM-CNR, c/o ESRF, Grenoble, France.

$Ce_{1-x}RE_xO_{2-x/2}$ compounds (RE= trivalent rare earth) are promising electrolytes for solid oxide fuel and electrolysis cells working at intermediate temperature. In such materials, crystallizing with a fluorite-type structure (F phase, *Fm*-3*m* space group), the ionic conductivity is particularly high at low dopant amounts, due to the partial substitution of Ce^{4+} by RE, which causes the formation of not-associated oxygen vacancies in the material. These vacancies are free to move through the F lattice, allowing the conduction of O^{2-} ions, thanks to a vacancies-hopping mechanism. However, the structural features ruling the ionic conductivity in such materials are quite complex, and a comprehensive structural study of doped ceria is therefore fundamental to evaluate which systems and compositions could be successfully employed in solid oxide cells [1, 2]. Recently, our research group performed a XAS study on the defects architecture in RE-doped ceria systems at the LISA beamline (BM08) of the ESRF synchrotron. The investigation focused on eight bulk samples belonging to the $Ce_{1-x}(Nd_{0.74}Tm_{0.26})_xO_{2-x/2}$ system [3] with $0.05 \leq x \leq 0.60$. We successfully collected both the EXAFS spectra of the samples at the Ce (40.4 keV), Nd (43.6 keV) and Tm (59.4 keV) K-edges, working in transmission conditions, and the XANES spectra at the L3-edges of the same elements (Ce= 5.7 keV, Nd= 6.2 keV and Tm= 8.6 keV), working in transmission and fluorescence modes.

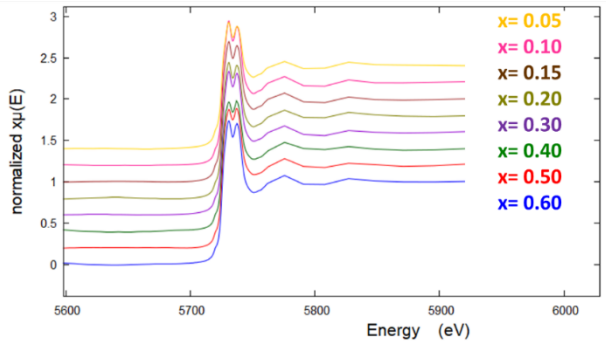

Figure 8 : Spectra collected at the Ce L3-edge on the considered samples, indicating the presence of Ce mainly in the 4+ oxidation state.

The investigation showed, as expected, a general increase in the structural disorder of the system with the increasing dopants amount, and the predominant presence of Ce in the $^{4+}$ oxidation state. Moreover, a sudden decrease in the interatomic distances is generally observed for the samples with $x \geq 0.3$, likely due to the predominant lattice contraction effect given by the oxygen vacancies formation: such compositional region matches the one in which a decrease in the ionic conductivity of these systems is generally observed.

[1] S. Presto *et al.*, *Phys. Chem. Chem. Phys.* **20**, 28338 (2018).

[2] C. Artini *et al., Energies* **13**, 1558 (2020).

[3] C. Artini *et al.*, *J. Energy Chem.* **60**, 494 (2021).

Local characterization of stoichiometrically-tailored WO_{3-x} thin films through XANES and EXAFS

H. Chen[1,2,3], S. M. Pietralunga[2,3], A. Puri[4], F. d'Acapito[4]

[1]Politecnico di Milano, [2]Institute for Photonics and Nanotechnologies (IFN)—National Research Council (CNR), [3]CNST@PoliMi, Istituto Italiano di Tecnologia (IIT), [4]CNR-IOM-OGG c/o ESRF, LISA CRG

The structure of tungsten oxide (WO_3) is complex and versatile, as WO_6 octahedrons can be at different distortion levels and can be stacked to form different structural phases. Additional presence of oxygen vacancies can make the structure even more complex while a good stability can be remained in normal conditions. Interesting properties, such as increasing electrical conductivity as a result of self-doping effect in sub-stoichiometric WO_{3-x}, arise in such a way that the tunability of properties is envisaged to be somehow controllable.

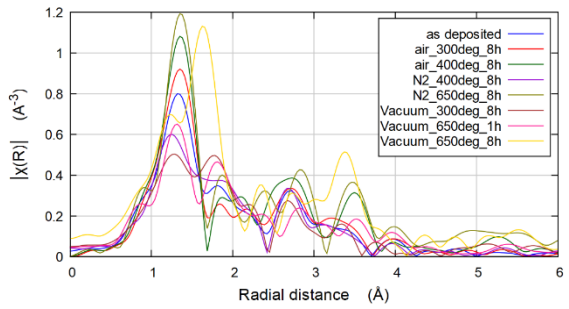

Figure 9: Fourier transformed radial distribution of differently pre-treated WO_{3-x} films from W L_3-edge EXAFS.

For the chase of a good understanding in differently structured and oxidized WO_{3-x}, WO_{3-x} films prepared through non-reactive RF-sputtering and subsequently annealing in different atmospheres, namely in dry air, nitrogen and vacuum, were examined by XANES and EXAFS measurements at the W-L_3 edge (at 10207 eV) in fluorescence mode. A grazing incidence angle was set between the focused X-ray beam and the film surfaces, respectively, 2 degrees for EXAFS and 45 degrees for XANES measurements.

The experiments were carried out at room temperature and in low vacuum. Figure 9 shows the Fourier transform of W-L_3 edge EXAFS spectra for differently pre-treated WO_{3-x} films, which present two different main W-O bonds within the first shell, and depending on the thermal treatments, the preference of the two main W-O bonds within the first shell is different. In addition, the peaks within radial distance (3~4 Å) start to appear for the WO_{3-x} films after crystallization was initiated by thermal treatments.

Scientific Highlights

Experimental evidence of palladium dissolution in anodes for alkaline direct ethanol and formate fuel cells

E.Berretti[1], M. V. Pagliaro[1], A.Giaccherini[2], G.Montegrossi[3], F.Di Benedetto[4], G.O. Lepore[5], F. d'Acapito[6] , F. Vizza[1] and A. Lavacchi[1]

[1] Institute for the Chemistry of Organometallic Compounds, Italian National Research Council (ICCOM-CNR), 50019 Florence, Italy. [2] Chemistry Department, University of Florence, 50019 Florence, Italy. [3] Institute of Geosciences and Earth Resources, Italian National Research Council (IGG-CNR), 50121 Florence, Italy. [4] Department of Earth Sciences, University of Ferrara, 44122 Ferrara, Italy. [5] Earth Sciences Department, University of Florence, 50121 Florence, Italy. [6] Istituto di Officina dei Materiali, Italian National Research Council (IOM-CNR), c/o European Synchrotron Radiation Facility (ESRF), Grenoble, France

Direct alcohol fuel cells (DAFCs) are considered as viable alternative for mid to low energy generation applications ; these systems share average output electrical powers, no need of ancillaire systems and the use of low-cost fuels which can be produced "greenly" by fermentation of agricultural products and waste biomasses. In this class of fuel cells, alcohol is fed in a liquid in the anodic compartment, while oxygen is supplied as gas in the cathodic compartment. Particularly, passive DAFCs represent a subclass suited for portable application and low temperatures, where oxygen is delivered by the air at the cathode, while a static tank is used as a reservoir for the alcoholic fuel at the anode. The main drawback of passive DAFCs, in the long-term runs, consists in the depletion of the fuelling species from the solution in the tank, leading to significant variations in the cell working potentials, and thus to an increased chance of degradation of the catalysts. In this context, platinum group metals (PGMs) are considered the best electrocatalytic materials for the reactions (both cathodic and anodic) that can be exploited in low-temperature alcohol fuel cells [1]. Due to PGMs cost and scarcity, the main challenge faced by researchers in the past few years was related to the decrease of precious metals loadings at the catalyst. Pt is still considered the prime choice catalyst for cathodic catalysts, while promising results were obtained with Porphyrin-like structures [2]. These M-N-C catalysts (M=Fe, Co) manifest a lower cost in respect to PGM catalysts with no potential losses due to fuel crossover, thanks to their oxygen-selective nature. Oppositely, effectiveness in anodic catalyst for alcohol electro-oxidation is still related to the adoption of PGMs [3]. Again, platinum is considered as the best catalyst for such reactions in acidic environment, while Palladium shows better activity towards alcohol oxidation in alkaline media [4,5]. The use of alkaline solutions could significantly improve FCs durability ; the acidic environment is responsible for the degradation processes of many of the cells' structural and functional components. The main issue related to the use of Pd as anodic catalyst is its deactivation, which leads to a loss in performance of the FCs in alkaline media [6,7]. During our pevious experiments, performed at LISA beamline [8,9], we studied in-situ the degradation of a Pd catalyst during anodic stress in alkaline electrolytes, using an half-cell electrochemical set-up. Adopting the Fixed Energy X-Ray Absorption Voltammetry (FEXRAV[10]) technique, we discovered that the deactivation in ethanol FCs was mainly due to dissolution of the catalyst. We also managed to define the different Pd species which were present in the system at the different potentials the electrode incurs. In this article we used FEXRAV to study the Pd behaviour in a real device (Figure 1), in order to asses if and when similar deactivation occurs. Particulary, we tested both an ethanol fuel cell, and a Formate fuel cell, showing a similar dissolution trend for the EtOH cell (Figure 2), and no dissolution for the formate one (Figure 3). These findings will be essential for a further technologization of such kind of fuel cells.

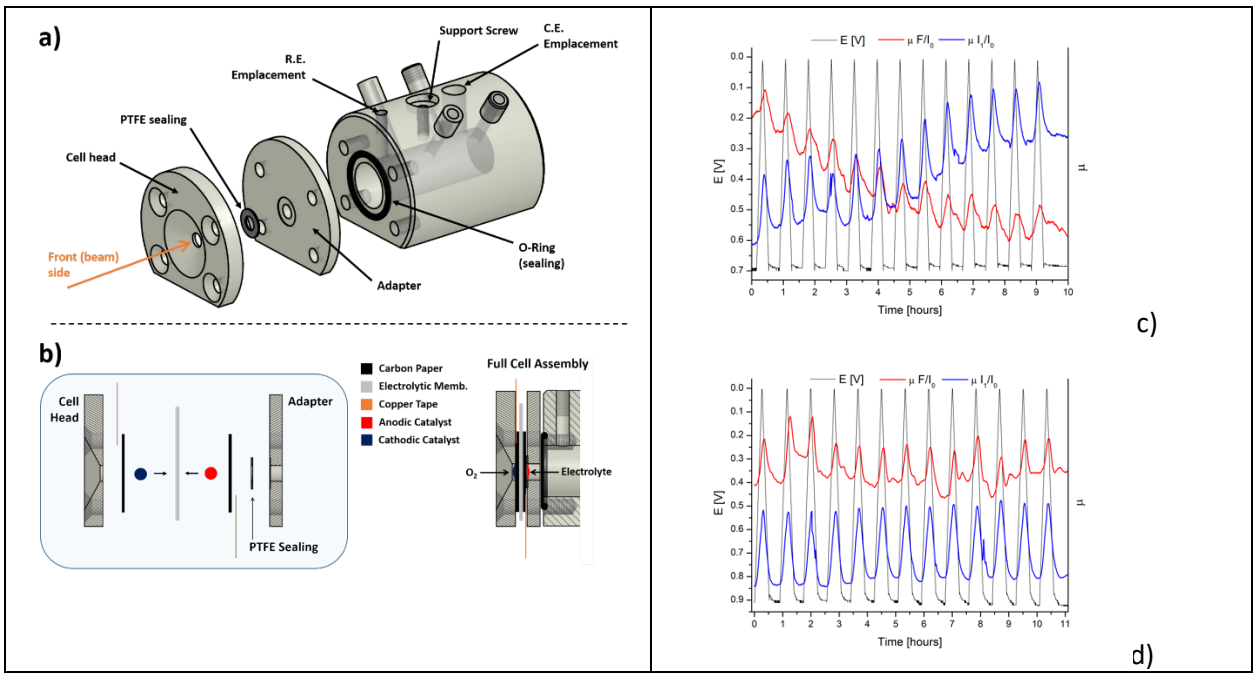

Figure 10: a, b)The FC assembly, c) – The FEXRAV of the EtOH FC, showing the dissolution of the Pd at the electrode (fluorescence signal,red curve) and the increase of the absorption signal in the bulk (transmission signal, blue curve), d)- The FEXRAV of the Formate FC, showing no dissolution (no change in signal between Transmitted, blue, and fluorescence, red, signals).

[1] A.M. Sheikh et al. Journal of Multidisciplinary Engineering Science and Technology. 1 (2014) 3159–40.

[2] E. Berretti et al. Current Opinion in Electrochemistry. 29 (2021) 100756.

[3] C. Lamy et al. Journal of Power Sources. 105 (2002) 283–296.

[4] L. Ma et al. International Journal of Hydrogen Energy. 37 (2012) 11185–11194.

[5] C. Bianchini et al. Chemical Reviews. 109 (2009) 4183–4206.

[6] L. Wang et al. Electrochimica Acta. (2015).

[7] E. Antolini et al. Journal of Power Sources. 195 (2010) 3431–3450.

[8] Berretti et al. Catalysts. 9 (2019) 659.

[9] G. Montegrossi et al. J Electrochem Soc. 164 (2017) E3690–E3695.

[10] A. Minguzzi et al. Anal Chem. 85 (2013) 7009–7013.

Publication: [Berretti et al. Electrochimica Acta 418, 140351-1-140351-9 (2022)]

Diffusion-driven formation of Co_3O_4 nanopetals layers for photoelectrochemical degradation of organophosphate pesticides

B. Kalinic[1], P. Ragonese[1], A. Faramawy[1], G. Mattei[1], M. Frasconi[2], R.Baretta[2], S. Bogialli[2], M. Roverso[2], G.A. Rizzi[2], C. Maurizio [1]

[1]Physics and Astronomy Department, University of Padova, Italy; [2]Department of Chemical Sciences, University of Padova, Italy

The results of an X-ray Absorption Spectroscopy experiment performed at the BM08 beamline of ESRF allowed to shed light on the formation mechanism of Co_3O_4 nanopetals on Si-based photoanodes by thermal oxidation of a deposited metallic film. This nanostructured layer has been then successfully employed in a photoelectrochemical experiment to detect and subsequently remove fenitrothion (FNT), a commonly used harmful organophosphate pesticide, which represents a serious risk to the public health.

The X-ray Absorption Spectroscopy (XAS) experiment was performed at the Co K-edge in fluorescence mode. The XAS spectra of crystalline powder pellets of Co_3O_4, CoO and the spectrum of a Co foil were collected in transmission mode as suitable references. The analysis of the XANES spectra was performed with a linear combination fit of the CoO, Co_3O_4 spectra and of the spectrum of an as-deposited metallic Co film. The EXAFS (Extended X-ray Absorption Fine Structure) analysis was performed with the FEFF8-IFEFFIT package.

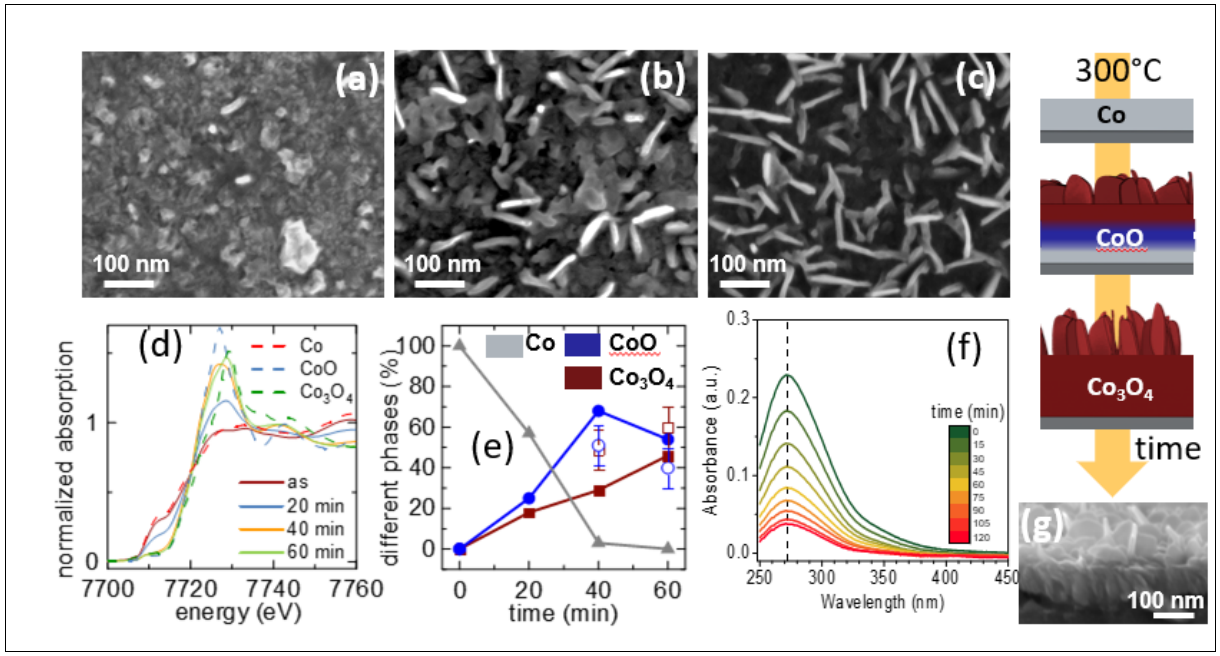

Figure 11: (a–c) SEM images of a 50 nm-thick Co deposited film annealed in air at 300 °C for 20 min (a), 40 min (b) and 60 min (c). (d) Normalized XANES spectra and (e) corresponding percentage of the different phases, as from XANES analysis. A sketch of the sample modification during annealing is drawn. The color code is the same as in (e). (f) UV–Vis spectra recorded at definite time intervals during the FNT photoelectrodegradation experiment, normalized to the buffer solution. (g) SEM image of the nanopetal layer (tilted view) at the end of the formation process.

The XAS analysis allowed to detect the different oxide phases progressively formed upon annealing (Figure 11 d-e). The analysis of the Co site upon different annealing conditions allowed to sketch the nanopetals formation mechanism (See Figure 11 a-c), that was debated in literature. The experimental results show that the petal formation is a mechanism induced by out-diffusion of Co atoms from the original film surface, rather than by a local melting, followed by subsequent oxidation (See sketch in Figure 11). They clarify that the petal formation requires a subtle equilibrium between the oxygen diffusion into the film and the non-uniform out-diffusion of Co atoms from the metallic film. Coupled to n-Si, Co_3O_4 nanopetals constitute an efficient photoanode for the photoelectrochemical detection of the organophosphate pesticide FNT, showing good sensitivity in a wide linear range, reproducibility and stability. The Si-Co_3O_4 nanopetals system also works very effectively for water remediation from organophosphate pesticides like FNT. Indeed, the photoelectrochemical production of hydroxyl radicals in a phosphate buffer solution, under visible light illumination, leads to a pesticide decomposition with a characteristic time of 1 h. Figure 11 (f) reports the UV-Vis absorption spectra of the solution during the process. This photoanode can be used several times, showing an excellent stability under working conditions, without any significant morphological or compositional surface change. These positive features, obtained with materials whose supply risk is at present not critical, and especially without using nanopowders, make this system highly promising for practical applications in contaminated water treatment.

Publication: [Applied surface Science, 596 (2022). 153552. DOI: 10.1016/j.apsusc.2022.153552]

Lanthanum captured in montmorillonite: evidence of inner-sphere complexes from X-ray Absorption Spectroscopy investigations

G.O. Lepore[1], E. Schingaro[2], E. Mesto[2], M. Lacalamita[2], C. Cristiani[3], P. Gallo Stampino[3], G. Dotelli[3], E. Finocchio[4], F. d'Acapito[5], G. Giuli[6]

[1]Dip. di Scienze della Terra - University of Florence, [2]Dip. di Scienze della Terra e Geoambientali - University of Bari, [3]Dip. di Chimica, Materiali e Ingegneria Chimica Giulio Natta, Politecnico dinMilano, [4]Dip. di Ingegneria Civile, Chimica e Ambientale, Università di Genova, [5]CNR-IOM-OGG c/o ESRF – The European Synchrotron, Grenoble, [6]Scuola di Scienze e Tecnologie-sez. geologia, Universitá degli Studi di Camerino

Tons of small Electrical and Electronic Equipment (WEEE) are disposed every year. The approach known as "urban mining", based on the development of recovery of precious materials from WEEE, bears then socioeconomic and environmental benefits. The study of efficient methods for metal recovery is therefore of clear interest. The solid/liquid adsorption process can remove metal ions from aqueous solutions with high efficiency and low costs, through a sustainable approach. The efficiency of the process is a key factor, and it depends on the adsorbent materials; thus, the study and development of solids with improved capability is crucial for the implementation at the industrial scale. In recent years, the feasibility of the use of pristine and modified clays for metal recovery has been reported [1], specifically the recovery of REs from aqueous solutions [2]. The capture/release results were interpreted in light of the interaction of the single ions with the solid sorbent, and on the basis of the physicochemical properties of the metal ions. Nonetheless, the mechanism of ion-sorbent interactions still needs to be fully clarified.

Here we report the results of an investigation on the performances of montmorillonites for the recovery of La ions from aqueous solutions. The study involves both the assessment of La uptake/release extent and structural investigations aimed at a deeper understanding of the process lying behind La incorporation. An X-Ray Absorption Spectroscopy study was performed at La L_3 edge on a set of montmorillonites: two source clays from the Clay Mineral Society repository in pristine form and a polymer-modified with a penta-etylen-hexamine of formula $C_{10}H_{28}N_6$. Ca- and Na-rich montmorillonite were previously contacted with La solutions of known initial concentration.

XAS results (Figure 12, left) evidence that La incorporation in the clay-based materials is independent on both polyamine presence and composition of the pristine clay. La-O distances for the first coordination shell range between 2.57 and 2.61 Å with coordination number with O atoms varying from 9 to 12.

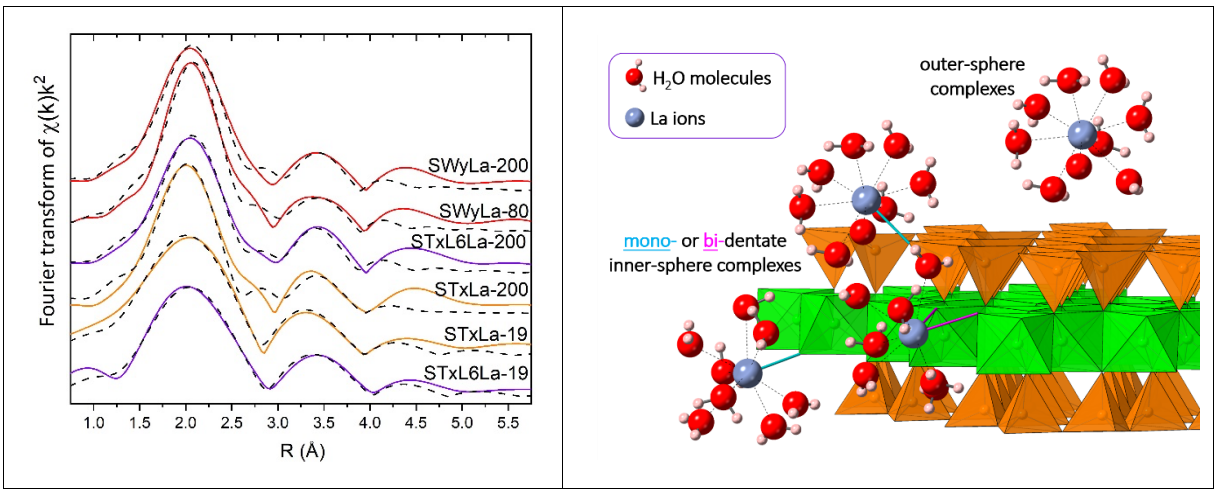

Figure 12 Left) EXAFS Fourier transform of the studied samples, plotted together with multiparameter fits (black dashed lines). Right) The TOT layers made of $AlO_4(OH)_2$ octahedra (green) and SiO_4 tetrahedra (orange) are negatively charged and neutrality is mainly provided by intercalation of hydrated cations in the interlayer. In the proposed inner-sphere complexation models, Red and blue-grey spheres are La and O atoms, respectively; light-blue and purple bars indicate corner-shared monodentate and bidentate complexes of La ions on octahedra and tetrahedra.

These results agree with the common interpretation that La incorporation occurs at the interlayer sites of the clays as an outer-sphere complex with water [3], thus without structural bonding of La inside the clay structure. However, our results also point out the presence of a further La-Si or La-Al distance (at ~ 4.1/-4.2 Å), indicating that a further incorporation mechanism must be considered. Indeed, La ions are likely at least partially adsorbed as inner-sphere complexes at the edges and/or at the surface of montmorillonite (Figure 12, right). The identification of this kind of interaction is of fundamental importance, since inner-sphere complexes are usually considered thermodynamically stable, thus playing an important role among the factors limiting the efficiency of the release process.

[1] C. Cristiani, M. Bellotto, G. Dotelli, S. Latorrata, G. Ramis, P. Gallo Stampino, E.M.I Zubiani, E. Finocchio *Minerals.* **2020**, *11*, 30.

[2] A. Munoz-Paez, M.D. Alba, R. Alvero, A.I. Becerro, M.A. Castro, J.M. Trillo *Phys. B: Condens. Matter* **1995**, *208*, 622-624.

[3] E. Padilla-Ortega, R. Leyva-Ramos, J. Mendoza-Barron, R.M Guerrero-Coronado, A. Jacobo-Azuara, A. Aragon-Piña, *Adsorp Sci Technol.* **2011**., *29*, 569-584.

Publication: [Appl. Clay Sci. **230** (2022), 106676.]

Unveiling the C position in $Mn_5Ge_3C_x$ thin films

L.-A. Michez[1], E. Prestat[2], F. d'Acapito[3], M. Petit[1], V. Heresanu[1], Q. Ramasse[3,2], V. Le Thanh[1], F. Boscherini[4], P. Pochet[5], M. Jamet[5]

[1]CINaM, Marseille, [2]SuperSTEM Lab., Daresbury, [3]CNR-IOM OGG c/o ESRF Grenoble, [4] Physics Department Bologna University, [5]CEA Grenoble

Heavily carbon-doped Mn_5Ge_3 is a unique compound for spintronics applications as it meets all the requirements for spin injection and detection in group-IV semiconductors. Despite the great improvement of the magnetic properties induced by C incorporation into the Mn_5Ge_3 compound, very little information is available on its structural properties and the genuine role played by C atoms.

In this work, we have used a combination of advanced complementary techniques to extensively characterize the structural and magnetic properties of $Mn_5Ge_3C_x$ films grown on Ge(111) by solid phase epitaxy as a function of C concentration. Our multiscale approach provides invaluable information on the C chemical environment and position in this complex material.

The C incorporation in the Mn_5Ge_3 matrix was first explored by extended x-ray absorption fine structure (EXAFS) spectroscopy at the K-edge of Mn on the BM08 beamline. Measurements were carried out on a model thin film of Mn_5Ge_3 and on thin films of $Mn_5Ge_3C_x$ with C doping x = 0.5 and x = 0.9. The related Fourier transforms of the EXAFS spectra collected are shown in Figure 13 (Left). The best fits were obtained using the hexagonal $P6_3/mcm$ structure of the Mn_5Ge_3 bulk material. The latter structure contains two crystallographically independent sets of manganese atoms, Mn_I and Mn_{II}, respectively (see inset of Fig. 1). Both sites exhibit a split first coordination shell with a component at roughly 2.50-2.60 Å (composed mostly of Ge neighbors, peak α in Figure 13) and the other at 2.95-3.02 Å (composed mostly of Mn neighbors, peak β). The EXAFS analysis, considering both sites with the two subshells, suggests that the C incorporation maintains the base structure of the cell as also shown by X-ray diffraction (XRD). It has a well visible effect on the configurational disorder of the second subshell that it is found to increase with C concentration in the thin films. On the other hand, a small contraction of the interatomic distances is detected with C addition considering the accuracy of the EXAFS analysis (about 1 %), which is consistent with the XRD analysis, in which a maximum cell contraction is found for x = 0.5.

As a complement of this atomic structure characterization performed as an average on the macroscopic scale, it is very important to carry out highly spatially resolved studies. The atomic arrangement in our films has been investigated using high-resolution scanning transmission-electron microscopy (HAADF-STEM) imaging in which each dot corresponds to a projected atomic column, with its brightness being related to the average atomic number over the whole projected column. The hexagonal structure of Mn_5Ge_3 is clearly visible in Figure 13 (right). To shed light on the position occupied by C, atomic resolution elemental maps were acquired using spatially resolved electron energy loss spectroscopy (EELS). The results are displayed in Figure 13 for Mn, Ge and C, respectively. The atoms occupy well-defined sites corresponding to the Wyckoff 4*d* and 6*g* for Mn and 6*g* for Ge, which is espected from the $P6_3/mcm$ crystal structure. For the first time, it is directly evidenced that C atoms occupy the Wyckoff 2*b* position at the center of the octahedral void.

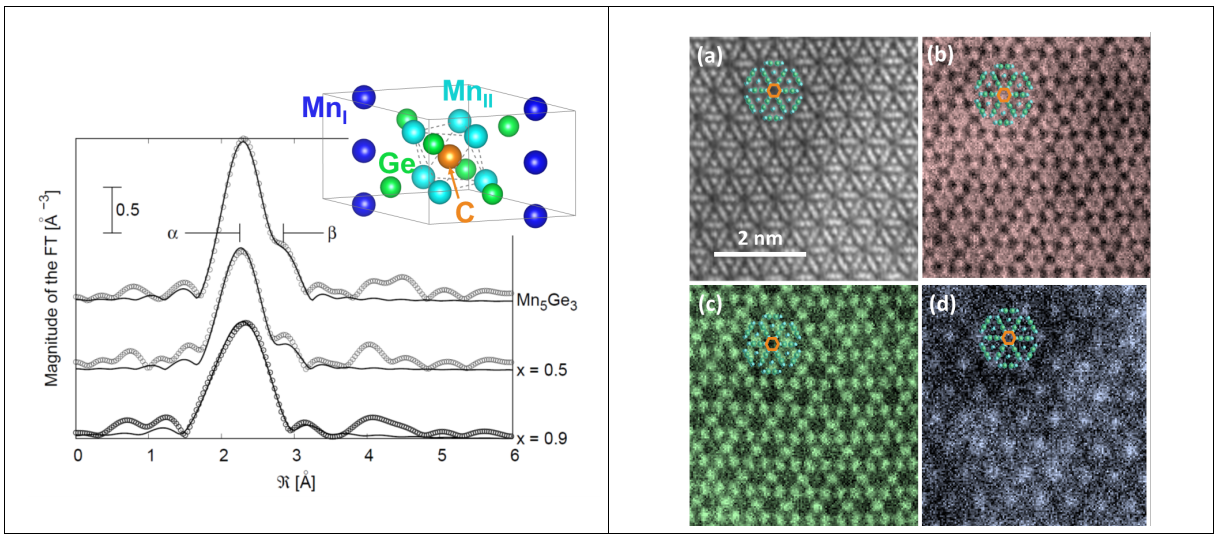

*Figure 13: **Left**: Fourier Transform modules of the EXAFS spectra measured on Mn_5Ge_3, $Mn_5Ge_3C_{0.5}$ and $Mn_5Ge_3C_{0.9}$ thin films. Points: experimental data, lines: fits. Crystal structure of Mn_5Ge_3 is presented on the top right corner. Colored spheres denote Mn (blue) and Ge (green) atoms. The C interstitial atom (in orange) fills one out the two octahedral sites corresponding to $Mn_5Ge_3C_{0.5}$ formula. **Right**: (a) HAADF STEM image and (b) to (d) the associated EELS elemental maps of a $Mn_5Ge_3C_{0.2}$ thin film at the Mn $L_{2,3}$- , Ge $L_{2,3}$- and C K-edges, respectively*

Accurate density functional theory (DFT) calculations support this result and draw an upper limit of occupancy to one out of the two sites per unit cell. The simulations are also consistent with the experimental observation of the reduction of the unit cell volume. In other words, $Mn_5Ge_3C_{0.5}$ is a stable ternary alloy and in this respect, is very similar to interstitially stabilized Nowotny phases.

This experimental finding indisputably confirms the C interstitial position that was considered in the magnetic properties calculations, which ascertains our understanding of the enhancement of the magnetic order: hybridization between Mn_{II} and C atoms takes place, which strengthens the exchange interaction between Mn_{II} atoms and thus, boosts the Curie temperature. This study provides therefore a complete picture of the structure of $Mn_5Ge_3C_x$ in thin films grown by solid phase epitaxy, bridging the gap between the structural and magnetic properties.

Publication: [Phys. Rev. Materials **6** (2022), 074404.]

Properties and conservation state of cadmium red ($CdS_{1-x}Se_x$) paints in twentieth century paintings by state-of-the-art techniques at multiple length scales

L. Monico [1], L. Cartechini [1], F. d'Acapito[2], A. Romani[1]

[1] CNR-SCITEC and Centre of Excellence SMAArt, c/o Department of Chemistry, Biology and Biotechnology, Perugia University, Italy, [2]CNR-IOM-OGG, c/o ESRF LISA CRG, Grenoble, France.

Cadmium red ($CdS_{1-x}Se_x$) is a class of 20th century artists' pigments featuring a tuneable shade from red-orange to red-purple with increasing selenium content. As direct band gap semiconductors, $CdS_{1-x}Se_x$ exhibit a distinctive luminescence both in the visible (near band edge emission, NBE) and in the NIR regions (deep level emissions, DLEs). The position of these emissions mainly depends on the selenium content, thus permitting to non-invasively distinguish among different varieties of cadmium reds in paintings. However, other factors than the Se content may influence the relative intensity of the DLE bands in cadmium reds spectra (Figure 14).

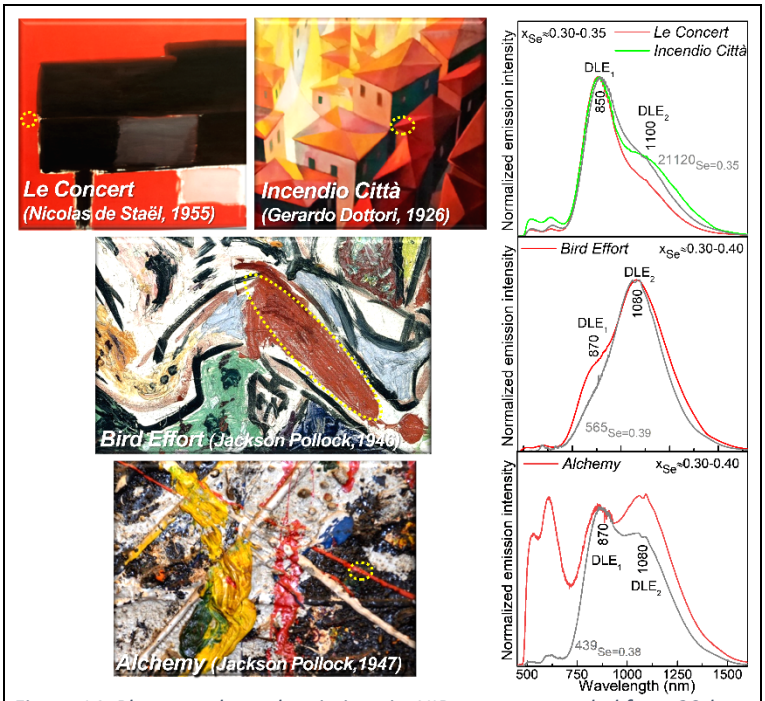

Figure 14: Photographs and emission vis–NIR spectra recorded from 20th century red paints composed of different CdS1−xSex pigments (red and green) compared to the ones of cadmium red reference compounds (grey).

Therefore, it is fundamental to gain insights on this aspect in order to assess how/if the intrinsic properties of the pigment may influence its (photo)chemical reactivity. In order to understand how some parameters related to intrinsic crystal defects of $CdS_{1-x}Se_x$, including its local atomic structure, influence the spectral properties of DLEs, we performed Se K-edge XAS investigations on selected couples of commercial and historical powders with a similar Se content (i.e., x~0.1: samples $21080_{Se=0.14}$ and $437_{Se=0.12}$; x~0.5: samples $21150_{Se=0.47}$ and $440_{Se=0.47}$) but DLEs with opposite relative intensities.

Se K-edge XANES spectral region (Figure 15-A the Se-poorer $21080_{Se=0.14}$/$437_{Se=0.12}$ and of the Se-richer $21150_{Se=0.47}$/$440_{Se=0.47}$ appear similar, meaning that no appreciable differences are visible between samples

with a similar selenium content. Only a slight shift towards lower energies of the maximum of the white line is visible with increasing selenium content. More revealing information are attainable by looking at the Se K-edge EXAFS spectra and the related Fourier Transforms (FT) in the 3–4 Å region (Figure 15-B), where a less pronounced second shell peak is present in the Se-richer pigments. The quantitative analysis of the Se K-edge XAS shows that the structure found is well described by the used fit model, that includes 4 Cd neighbours at 2.60 Å, a mixed (S,Se) second shell at 4.16 Å and a third shell of Cd atoms at 5.05–5.10 Å. The Se-poorer $21080_{Se=0.14}$/$437_{Se=0.12}$ and the Se-richer $21150_{Se=0.47}$/$440_{Se=0.47}$ share the same parameters, meaning that pigments with a comparable selenium content have an identical local environment. In line with XRPD and EDX results (not show here), the former pair is almost pure CdS, whereas the latter pair exhibits a content of Se of ca. 0.4.

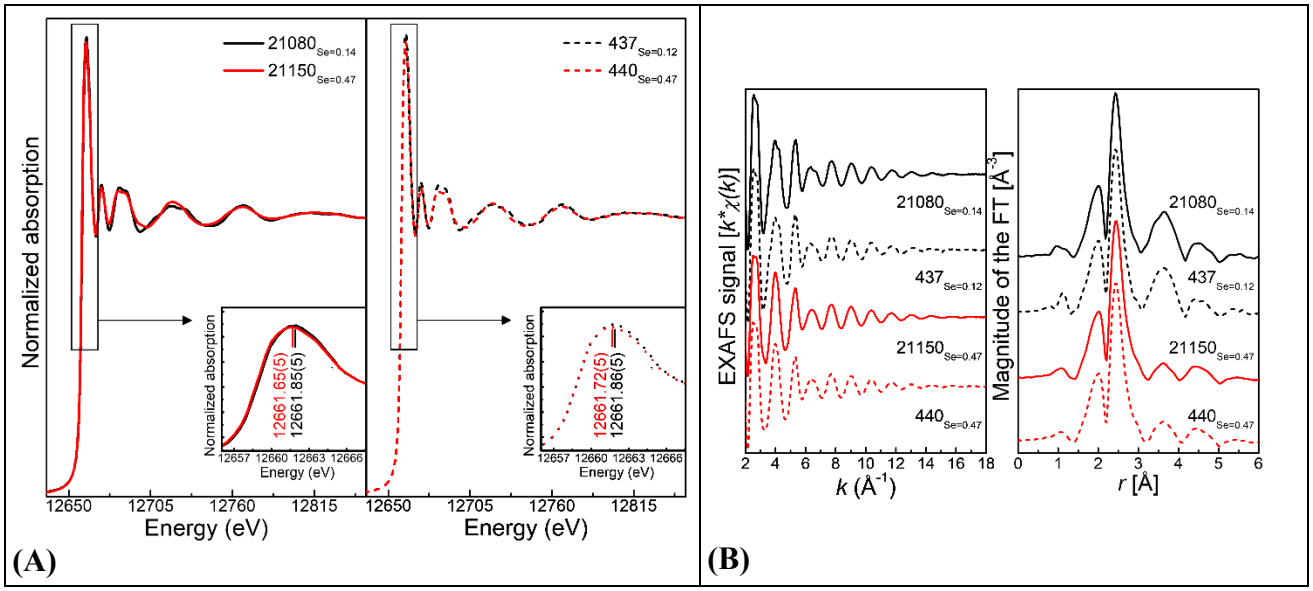

Figure 15 (A) Se K-edge XANES spectra and (B) k-weighted Se K-edge EXAFS spectra in k space with corresponding FT in the range k =[2–16] Å^{-1} of commercial (solid line) and historical (dotted line) $CdS_{1-x}Se_x$ pigment powders.*

To summarize, Se K-edge XAS results show that the local atomic structure of $CdS_{1-x}Se_x$ depend only on the selenium content and, for a specific x value, cannot be correlated with the changes observed in the positions of the DLE bands and in their relative intensity.

The results from pigment powders, integrated with those obtained from equivalent artificially aged oil paint mock-ups, revealed that changes in the spectral properties of DLEs appear instead to be influenced by the presence of moisture. Such findings have opened the way for targeted research on the main intrinsic factors and other external parameters related to the manufacturing process of cadmium reds that may affect the characteristic vis–NIR photoluminescence of $CdS_{1-x}Se_x$ with a similar selenium abundance and any eventual correlation with their (photo)-chemical reactivity.

Publication: [European Physical Journal Plus **137** (2022) 311]

Year 2022 publications

1. Berretti E., Pagliaro M.V., Giaccherini A., Montegrossi G., Di Benedetto F., Lepore G.O., d'Acapito F., Vizza F., Lavacchi A. - Experimental evidence of palladium dissolution in anodes for alkaline direct ethanol and formate fuel cells Electrochimica Acta 418, 140351-1-140351-9 (2022).
2. Dalebout R., Barberis L., Totarella G., Turner S.J., La Fontaine C., de Groot F.M.F., Carrier X., van der Eerden A.M.J., Meirer F., de Jongh P.E. - Insight into the nature of the ZnO_x promoter during methanol synthesis ACS Catalysis 12, 6628-6639 (2022).
3. Das A., Balasubramanian C., Orpe P., Pugliese G.M., Puri A., Marcelli A., Saini N.L. - Morphological, electronic, and magnetic properties of multicomponent cobalt oxide nanoparticles synthesized by high temperature arc plasma Nanotechnology 33, 095603-1-095603-13 (2022).
4. Fantin A., Cakir C.T., Kasatikov S., Schumacher G., Manzoni A.M. - Effects of heat treatment on microstructure, hardness and local structure in a compositionally complex alloy Materials Chemistry and Physics 276, 125432-1-125432-6 (2022).
5. Kalinic B., Girardi L., Ragonese P., Faramawy A., Mattei G., Frasconi M., Baretta R., Bogialli S., Roverso M., Rizzi G.A., Maurizio C. - Diffusion-driven formation of Co_3O_4 nanopetals layers for photoelectrochemical degradation of organophosphate pesticides Applied Surface Science 596, 153552-1-153552-9 (2022).
6. Koeberl C., Glass B.P., Schulz T., Wegner W., Giuli G., Cicconi M.R., Trapananti A., Stabile P., Cestelli-Guidi M., Park J., Herzog G.F., Caffee M.W. - Tektite glasses from Belize, Central America: Petrography, geochemistry, and search for a possible meteoritic component Geochimica et Cosmochimica Acta 325, 232-257 (2022).
7. Lepore G.O., Schingaro E., Mesto E., Lacalamita M., Cristiani C., Gallo Stampino P., Dotelli G., Finocchio E., d'Acapito F., Giuli G. - Lanthanum captured in montmorillonite: Evidence of inner-sphere complexes from X-ray Absorption Spectroscopy investigations Applied Clay Science 230, 106676-1-106676-7 (2022).
8. Menushenkov A.P., Ivanov A.A., Chernysheva O.V., Rudnev I.A., Osipov M.A., Kaul A.R., Chepikov V.N., Mathon O., Monteseguro V., d'Acapito F., Puri A. - The influence of $BaSnO_3$ and $BaZrO_3$ nanoinclusions on the critical current and local structure of HTS coated conductors Superconductor Science and Technology 35, 065006-1-065006-9 (2022).
9. Michez L.A., Petit M., Heresanu V., Le Thanh V., Prestat E., d'Acapito F., Ramasse Q., Boscherini F., Pochet P., Jamet M. - Unveiling the atomic position of C in $Mn_5Ge_3C_x$ thin films. Physical Review Materials 6, 074404-1-074404-13 (2022).
10. Monico L., Rosi F., Vivani R., Cartechini L., Janssens K., Gauquelin N., Chezganov D., Verbeeck J., Cotte M., d'Acapito F., Barni L., Grazia C., Buemi L.P., Andral J.L., Miliani C., Romani A. - Deeper insights into the photoluminescence properties and (photo)chemical reactivity of cadmium red ($CdS_{1-x}Se_x$) paints in renowned twentieth century paintings by state-of-the-art investigations at multiple length scales European Physical Journal Plus 137, 311-1-311-21 (2022).
11. Pipitone C., Carlotto S., Casarin M., Longo A., Martorana A., Giannici F. - Bi^{3+} doping in 1D $((CH_3)(3)SO)PbI_3$: A model for defect interactions in halide perovskites Journal of Materials Chemistry C 10, 1458-1469 (2022).
12. Preeti, Naidu K.L., Krishna M.G., Mohiddon M.A. - Investigation of crystallographic changes across the Cr/a-Si interface by X-ray absorption spectroscopy Applied Surface Science 592, 153204-1-153204-8 (2022).

Contacts

Beamline responsible:

Francesco d'Acapito: dacapito@esrf.fr , +33 4 7688 2426, +33 6 8936 4302

Beamline scientists:

Alessandro Puri: puri@esrf.fr , +33 4 7688 2859

Administration:

Fabrizio La Manna, lamanna@esrf.fr , +33 4 7688 2962

Beamline: +33 4 7688 2085

Laboratory: +33 4 7688 2743

Skype: LISA_beamline@EBS

Web page: http://www.esrf.eu/UsersAndScience/Experiments/CRG/BM08/

Forthcoming proposals submission deadlines

ESRF quota: March 1st 2023

CERIC quota: early 2023, date to be announced

Contributors to this issue

F. d'Acapito, M. Brunelli & A. Puri (CNR-IOM, Grenoble), D. Benedetti (CNR-IOM, Trieste), H. Chen (Politecnico Milano), X. He (Univ. Milano Statale), S. Massardo (Univ. Genova), F. Bardelli (CNR-NANOTEC, Roma), E. Berretti (CNR-ICCOM, Firenze), G. O. Lepore (Univ. Firenze), C. Maurizio (Univ. Padova), L. Michez (Univ. Marseille), L. Monico, L. Cartechini & A. Romani (CNR-ISTEC, Perugia).